J. Iron Steel Res. Int. (2022) 29:1723–1733
https://doi.org/10.1007/s42243-022-00827-y

ORIGINAL PAPER

Kinetics and mechanism of coal-based direct reduction of high-chromium vanadium–titanium magnetite

Jian Yang[1] · Tao Jiang[2] · Shi-hong Ma[2] · Song-tao Yang[3] · Mi Zhou[2]

Received: 12 October 2021 / Revised: 13 December 2021 / Accepted: 17 December 2021 / Published online: 5 October 2022

Abstract

High-chromium vanadium–titanium magnetite (HCVTM) is a valuable resource containing metal elements such as iron, vanadium, titanium, and chromium. To recycle these elements, direct reduction is an efficient way. The mechanism and reaction kinetic parameters for the direct reduction of HCVTM were studied. Experimental results show that the reduction degree increases obviously when the C/O ratio and temperature increase. Thermodynamic analysis showed a dramatic mass loss in the direct reduction of HCVTM in the temperature range of 985–1160 °C. From 1200 to 1350 °C, the reduction curves for the isothermal reduction of HCVTM followed the same trend, with a sharp increase in the initial reaction zone and a slight increase in the reduction rate with increasing time, and finally, the isothermal reduction process of HCVTM was divided into several limiting stages with varying degrees, with inconsistent limiting factors for the reaction rate at different stages. The results also show that the activation energy decreases slightly at larger degrees of reduction. Also, the apparent rate constant $k(T)$ increased with increasing reduction temperature, with $\ln k(T)$ showing a good linear relationship with temperature.

Keywords High-chromium vanadium–titanium magnetite · Direct reduction · Reduction rate · Kinetic · Thermodynamic analysis

1 Introduction

Vanadium–titanium magnetite is a kind of iron ore that contains titanium (Ti) and vanadium (V) mainly, combined with a small amount of chromium (Cr), gallium (Ga), scandium (Sc), cobalt (Co), nickel (Ni), platinum (Pt), and other components [1, 2]. It is present as V, Ti, and Fe in a symbiotic form. Thus, it is called vanadium titanomagnetite [3]. It can be classified into two categories due to the amount of Cr_2O_3 contained: the ordinary vanadium–titanium magnetite and high-chromium vanadium–titanium magnetite (HCVTM). The world's vanadium and titanium magnetite resources are mainly distributed in Russia, South Africa, China, the USA, Canada, Norway, Finland, Sweden, India, Australia, and New Zealand, and the world reserves are nearly 48 billion tons [4]. In China, it is mainly deposited in the Panxi area, Sichuan province. Hongge in the Panzhihua–Xichang area has the highest reserves (up to 3.6 billion tons). In this area, vanadium titanomagnetite belongs to HCVTM, and it has a high value of comprehensive utilization [5]. The main phase in HCVTM is magnetite (Fe_3O_4), ilmenite ($FeTiO_3$), and chromite ($FeCr_2O_4$). V in HCVTM is mainly in the phase of FeV_2O_4. HCVTM is a good valuable resource with high iron content. Iron (Fe), vanadium, titanium, and chromium are recognized as important strategic resources all over the world.

Over the years, metallurgical researchers have conducted a lot of research on the comprehensive utilization of vanadium–titanium magnetite concentrate [6–12]. Based on the characteristics of these methods, the typical methods can be divided into two categories: blast furnace method and non-blast furnace methods [6]. By blast furnace

✉ Mi Zhou
zhoumineu@163.com

[1] School of Information Science and Engineering, Northeastern University, Shenyang 110819, Liaoning, China

[2] School of Metallurgy, Northeastern University, Shenyang 110819, Liaoning, China

[3] School of Materials and Metallurgy, University of Science and Technology Liaoning, Anshan 114051, Liaoning, China

method, metals are recovered by using the blast furnace and converter furnace. It can realize the recovery of iron and vanadium in vanadium–titanium magnetite concentrate [7, 8]. However, most Ti enters the slag by this method, which has an influence on the performance of building materials to produce slag cement as raw material.

Non-blast furnace methods include the rotary kiln–electric furnace method, reduction–grinding method, and sodium-extracted vanadium–rotary kiln–electric furnace method [13]. The rotary kiln–electric furnace method needs to meet the high operational control requirements. The reduction–grinding method required a high metallization ratio and grain size of ores. By sodium-extracted vanadium–rotary kiln–electric furnace method, HCl, Cl_2, SO_2, SO_3, and other gases will corrode the equipment during the sodium roasting process.

In recent years, coal-based direct reduction of vanadium titanomagnetite has been studied broadly to achieve the efficient separation and comprehensive utilization of Fe, V, Ti, Cr, and other resources [7, 14–18]. The research involves the effects of carbon distribution, reduction temperature, reduction time, reduction atmosphere, raw material particle size, and pellet size on the direct reduction characteristics of vanadium–titanium magnetite concentrate. The process parameters of direct reduction of coal-based pellets are optimized under laboratory conditions [15, 19–23].

Rotary hearth furnace direct reduction technology was proposed to reduce vanadium–titanium magnetite concentrate, and the orthogonal experiment method was employed to study the effects of C/O ratio, roasting time, and roasting temperature on metallization ratio and compressive strength [24]. The results showed that the C/O ratio of 1.3, the roasting temperature of 1330 °C, and the roasting time of 25 min were the optimal experiment scheme. In an experiment performed by Chen et al. [22], the process of metalizing reduction and magnetic separation for vanadium titanomagnetite was proposed. The recovery ratios of Fe, V, and Ti were 91.19%, 61.82%, and 85.31%, respectively. In the study of Zhao et al. [15], most of V, Cr, and Ti were concentrated into slag by the process of coal-based reduction–magnetic separation for HCVTM. The recovery ratios of V, Cr, and Ti were only about 40%, 80%, and 20%, respectively.

Liu et al. [25] carried out high-temperature experiment in a furnace at 1350 °C. In N_2 atmosphere, carbon-containing pellets were reduced for different time, and the composition and microstructure of carbon-containing pellets were analyzed by thermogravimetry (TG), differential scanning calorimetry (DSC), X-ray diffraction (XRD), and scanning electron microscopy (SEM). The experimental results show that the reduction process of vanadium–titanium concentrate is Fe_2TiO_4 and Fe_3O_4, $3Fe_3O_4{\cdot}Fe_2TiO_4$, $Fe_3O_4{\cdot}Fe_2TiO_4$, Fe_2TiO_4, FeO, and Fe.

Liu et al. [26] also carried out a direct reduction experiment of vanadium–titanium iron concentrate. The reaction process was developed into two stages: the initial stage of reduction and the final stage of reduction. The reaction activation energy of the initial stage was 73.17 kJ/mol, and the reaction activation energy of the final stage was 152.02 kJ/mol. The reaction speed at the final stage of reduction was lower than that at the initial stage.

Besides, in a study performed by Ding et al. [27], vanadium–titanium magnetite concentrate was directly reduced and smelting-separated isothermally with graphite and $CaCO_3$. The influences of basicity and cooling technique on reduction and smelting separation were studied. In the study of Sun et al. [28], the effective separation of slag and metal phases could be obtained in which over 95% Fe was transferred into metal phase and over 90% Ti was remained in slag. The effects of molar ratio of C to Fe n(C)/n(Fe) and temperature on the behavior of vanadium and chromium during direct reduction and magnetic separation were investigated in another study performed by Zhao et al. [15]. These studies mainly focus on the optimization of direct reduction and smelting separation operation parameters and investigate the effects of temperature and time on the reduction rate and metal recovery of vanadium–titanium magnetite.

In this paper, the mechanism and reaction kinetic parameters of the direct reduction of a high-chromium vanadium–titanium magnetite from western China are investigated. Due to the existence of chromium, the reduction kinetics and mechanism of this mineral need to be further analyzed, which is also the original intention of this paper. In order to understand the reaction rate, the effects of various factors on the reaction rate, the restrictive step in the reaction process, and the reaction mechanism are investigated. It is necessary to study the reaction kinetics of HCVTM. Isothermal kinetics of direct reduction of HCVTM is developed by the thermogravimetric method. The research contains calculation of kinetic mechanism function and kinetic parameters, coal-based direct reduction kinetic model, and mechanism of the reaction. It is expected to select proper reduction conditions, control the reduction reaction, and optimize the reduction process.

2 Experimental

2.1 Materials

To investigate the direct reduction characteristic of HCVTM, the reduction experiments were carried out by

Table 1 Chemical composition of HCVTM concentrate (wt.%)

TFe	FeO	TiO_2	SiO_2	Al_2O_3	MgO	CaO	V_2O_5	Cr_2O_3	P	S
50.16	26.47	12.44	4.60	2.58	3.68	0.48	0.57	1.28	< 0.01	0.15

Table 2 Composition of coal (wt.%)

Fixed carbon	Volatile	Moisture	S	P	Ash				
					FeO	CaO	MgO	SiO_2	Al_2O_3
78.62	6.80	2.74	0.67	0.04	0.56	0.37	0.15	5.97	4.08

Table 3 Distribution of particle size of ore and coal

Particle size/μm	≤ 0.5000	≤ 1.000	≤ 2.000	≤ 5.000	≤ 10.00	≤ 20.00	≤ 45.00	≤ 75.00	≤ 100.0	≤ 200.0
Ratio in ore/%	26.54	27.76	37.40	67.86	87.17	96.81	100	100	100	100
Ratio in coal/%	11.19	11.83	16.91	36.96	54.01	66.38	78.02	89.13	95.89	100

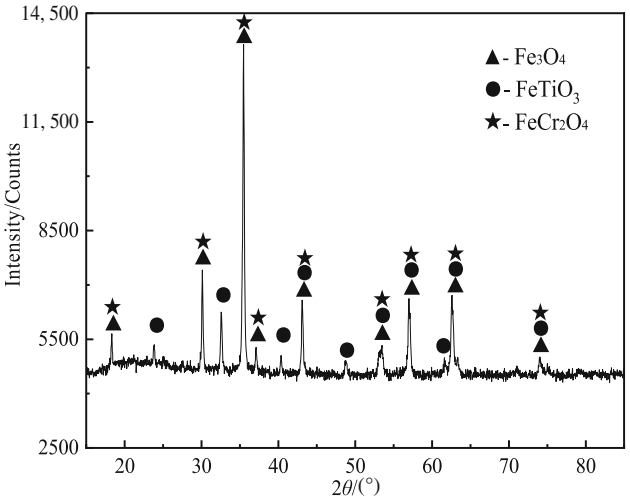

Fig. 1 XRD pattern of HCVTM concentrate. 2θ—Diffraction angle

using a reduction furnace. The sample in the experiment was a mixture of coal and HCVTM. The main contents of coal and HCVTM are shown in Tables 1 and 2, and the particle sizes of the ore and the coal are listed in Table 3, which are tested using a laser particle size analyzer BT6300. The phases of raw materials were identified with an X-ray diffractometer. Figure 1 presents the XRD patterns of HCVTM concentrate before the reduction reaction. It indicates that the main phases in HCVTM are magnetite (Fe_3O_4), ilmenite ($FeTiO_3$), and chromite ($FeCr_2O_4$).

At experimental temperature, the reduction reaction of Ti oxide could not occur. Contents of V_2O_5 and Cr_2O_3 are merely 0.57% and 1.28%, respectively. Therefore, the content of iron in HCVTM was used to calculate the amount of theoretical carbon content. The molar ratios of oxygen atoms in iron oxides and fixed carbon in coal powder were calculated. The calculation formula is as follows:

$$W_{Fe_2O_3} = \left(W_{TFe} - W_{FeO} \times \frac{M_{Fe}}{M_{FeO}}\right) \times \frac{M_{Fe_2O_3}}{2M_{Fe}} \quad (1)$$

where W is the mass content of components in HCVTM, %; and M is the molar mass of components, g/mol. In this paper, 100 g HCVTM was taken as an example for calculation, and the mass of FeO and Fe_2O_3 is 26.47 and 42.25 g, respectively. The mole of oxygen n(O) is 1.1598 mol. Composition of the sample at different carbon to oxygen ratios is shown in Table 4.

2.2 Experimental apparatus and methods

Before experiments, HCVTM and coal were dried for 24 h. The HCVTM and coal were then placed in a ball mill tank and ground for 10 h so that they were less than 74 μm in size. In the mill tank, as a binder, vinol was mixed with coal and HCVTM. By pressure forming equipment, a carbon-bearing pellet was prepared with pressure of 35 MPa. The compressed sample is a 21 mm × 19 mm × 13 mm ellipsoid pellet, as shown in Fig. 2. The prepared carbon-bearing pellet was put into the drying oven under 110 °C for 6 h.

Table 4 Composition of sample at different C/O ratios

C/O	Coal/g	HCVTM/g
0.7	12.39	100
0.8	14.16	100
0.9	15.93	100
1.0	17.70	100
1.1	19.47	100
1.2	21.24	100
1.3	23.01	100

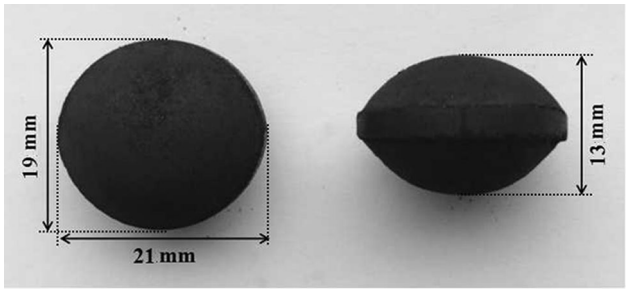

Fig. 2 Carbon-bearing pellet

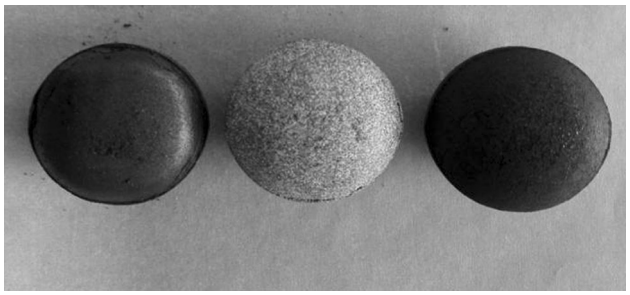

Fig. 3 Three kinds of pellets

A high-temperature tubular furnace was used in this experiment. The furnace was heated at a heating rate of 10 °C/min. When the temperature reached the setting temperature (1200, 1250, 1300, and 1350 °C), N_2 was input to provide an inert atmosphere. The mass flow rate of N_2 is 1 L/min. The temperature was kept for 10 min. Then, the hanging basket was put into the furnace tube and suspended by nickel chromium alloy wire at the bottom of the electronic balance on the upper part of the furnace cover. The mass of pellet was analyzed every 30 s. The temperature was controlled by the precision of 0.5 °C, and the measurement error of the balance was 0.0001 g. After 30 min, the sample was quickly taken out and put into a nitrogen reactor for cooling. After the sample was completely cooled, the sample was taken out and ground to 74 μm, and then, its metallization ratio was calculated based on chemical analysis.

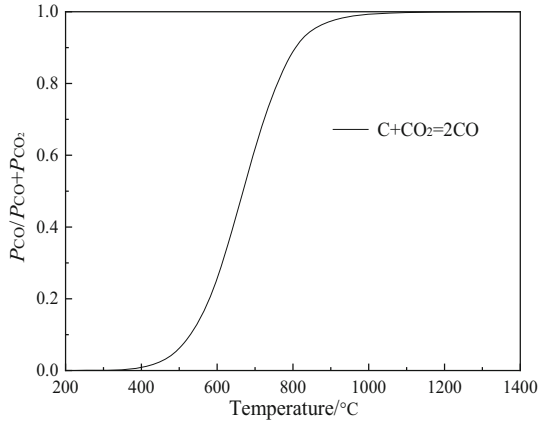

Fig. 4 Equilibrium curve of carbon gasification. P_{CO}—CO partial pressure; P_{CO_2}—CO_2 partial pressure

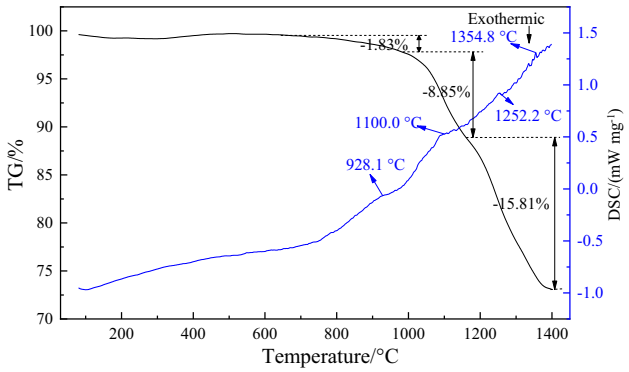

Fig. 5 TG–DSC curves of mixture of HCVTM and coal

2.3 Determination of reduction degree of HCVTM

By the thermogravimetry method, the reduction degree of HCVTM is calculated at 1200, 1250, 1300, and 1350 °C, respectively. In this experiment, all data are acquired in isothermal reduction conditions. Based on the analysis of the mass loss of samples, the reduction degree is calculated. The reduction degree R_t is defined by the following formula:

$$R_t = \frac{\Delta m_O^t}{\Delta m_O^0} \tag{2}$$

where R_t is the reduction degree at time t, s; Δm_O^t is the mass loss of oxygen at time t, g; Δm_O^0 is the total mass of oxygen in HCVTM, g, $\Delta m_O^0 = 0.18557 m_0$; and m_0 is the initial mass of HCVTM, g.

The mass loss of reduction oxygen and fixed carbon from coal can be calculated by:

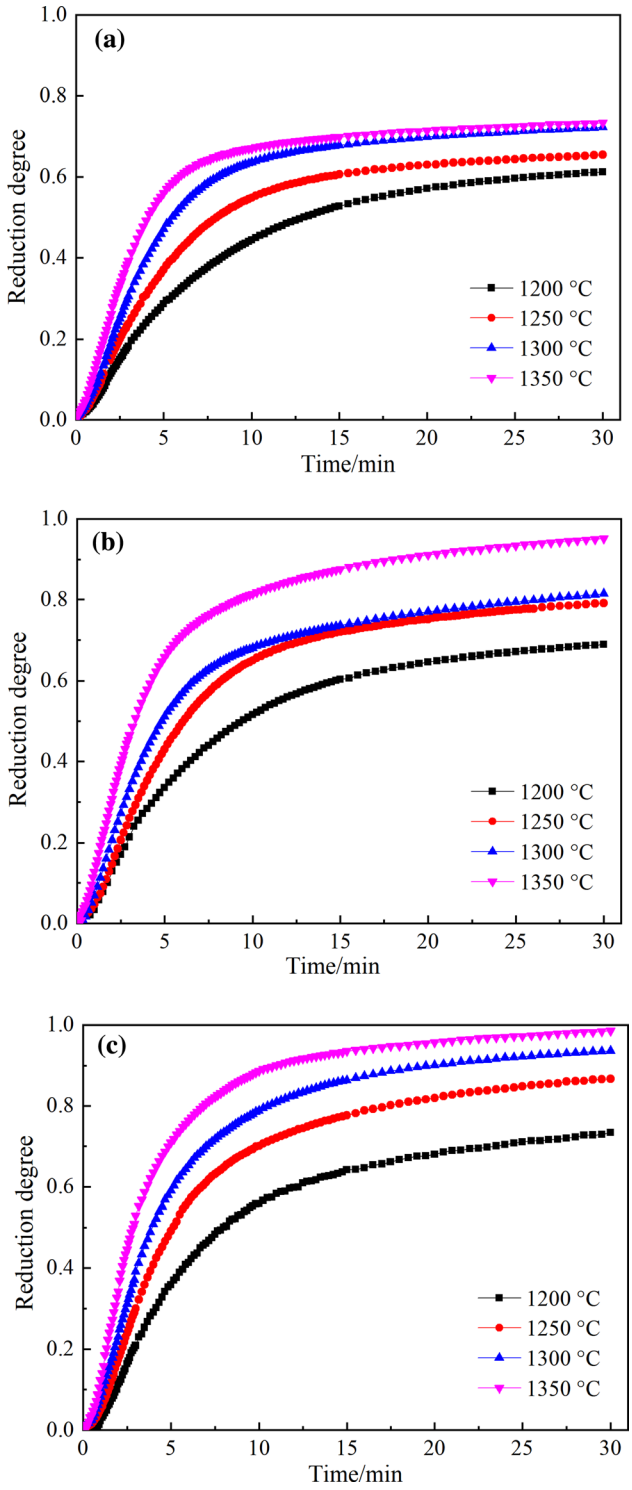

Fig. 6 Reduction degree of HCVTM with different C/O ratios. **a** C/O = 0.6; **b** C/O = 1.0; **c** C/O = 1.4

$$\Delta m_t = \Delta m_{\Sigma}^t - \Delta m_{\mathrm{V}}^t - \Delta m_{\mathrm{M}}^t \quad (3)$$

where Δm_t is the mass loss of reduction oxygen and fixed carbon at time t, g; Δm_{Σ}^t is the total mass loss of sample mixture at time t, g; Δm_{V}^t is the mass loss of volatiles and water at time t, g; and Δm_{M}^t is the mass loss of heating process of iron ore, g. To determine the mass loss percentage of the sample, three kinds of pellets were prepared in the experiment. Pellet (1) is carbon-bearing HCVTM pellet, pellet (2) is carbon-bearing Al_2O_3 pellet, and pellet (3) is vanadium–titanium magnetite pellet. The coal mass in three kinds of pellets is equal. A picture of three kinds of pellets is shown in Fig. 3.

The curve of carbon gasification is shown in Fig. 4, when the temperature is higher than 1100 °C and the partial pressure of CO is close to 1. Thus, the direct reduction by CO can be neglected when the temperature is higher than 1100 °C. In the reduction process, reduction oxygen and fixed carbon are both output in the form of CO. Thus, the reduction oxygen mass loss at time t is as follows.

Table 5 Differential and integral expressions of common reaction mechanism functions

Code	Reaction model	Differential $f(\alpha)$	Integral $G(\alpha)$
1	A_1	$1-\alpha$	$-\ln(1-\alpha)$
2	$A_{3/2}$	$\frac{3}{2}(1-\alpha)[-\ln(1-\alpha)]^{\frac{1}{3}}$	$[-\ln(1-\alpha)]^{\frac{2}{3}}$
3	$A_{1/2}$	$\frac{1}{2}(1-\alpha)[-\ln(1-\alpha)]^{-1}$	$[-\ln(1-\alpha)]^2$
4	R_2	$2(1-\alpha)^{\frac{1}{2}}$	$1-(1-\alpha)^{\frac{1}{2}}$
5	R_3	$3(1-\alpha)^{\frac{2}{3}}$	$1-(1-\alpha)^{\frac{1}{3}}$
6	D_6	$\frac{3}{2}(1-\alpha)^{\frac{2}{3}}\left[1-(1-\alpha)^{\frac{1}{3}}\right]^{-1}$	$\left[1-(1-\alpha)^{\frac{1}{3}}\right]^2$
7	D_8	$\frac{3}{2}\left[(1-\alpha)^{-\frac{1}{3}}-1\right]^{-1}$	$1-\frac{2}{3}\alpha-(1-\alpha)^{\frac{2}{3}}$

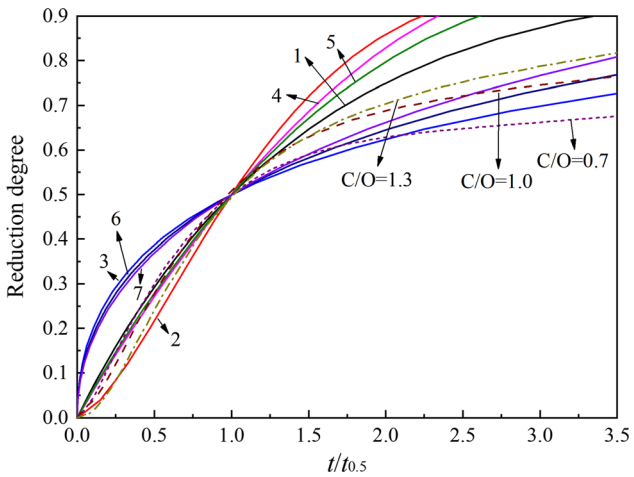

Fig. 7 Relationship between reduction degree and dimensionless reduction time

$$\Delta m_{\mathrm{O}}^{t} = \frac{16}{28}\Delta m_t \tag{4}$$

When Eqs. (3) and (4) are substituted in Eq. (2), R_t is obtained as Eq. (5).

$$R_t = \frac{\frac{16}{28}\left(\Delta m_{\Sigma}^{t} - \Delta m_{\mathrm{V}}^{t} - \Delta m_{\mathrm{M}}^{t}\right)}{0.18557 m_0} \tag{5}$$

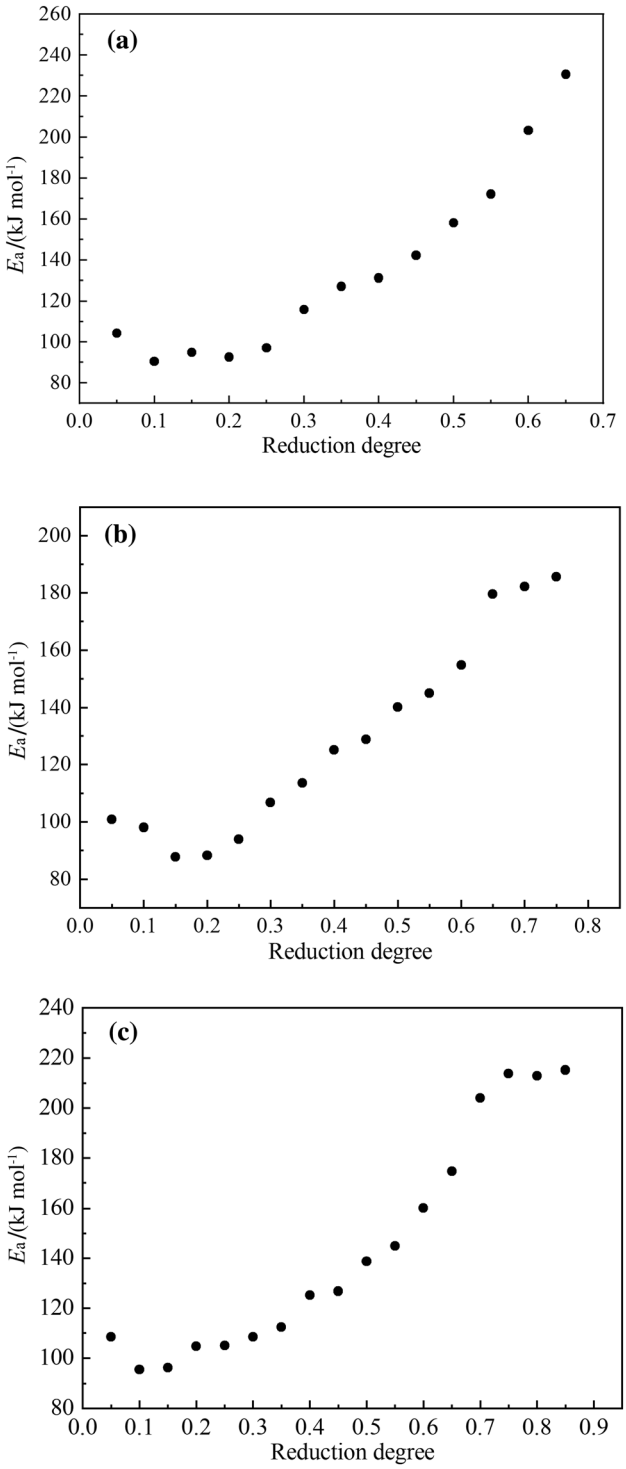

Fig. 8 Relationship between activation energy and reduction degree. **a** C/O = 0.7; **b** C/O = 1.0; **c** C/O = 1.3

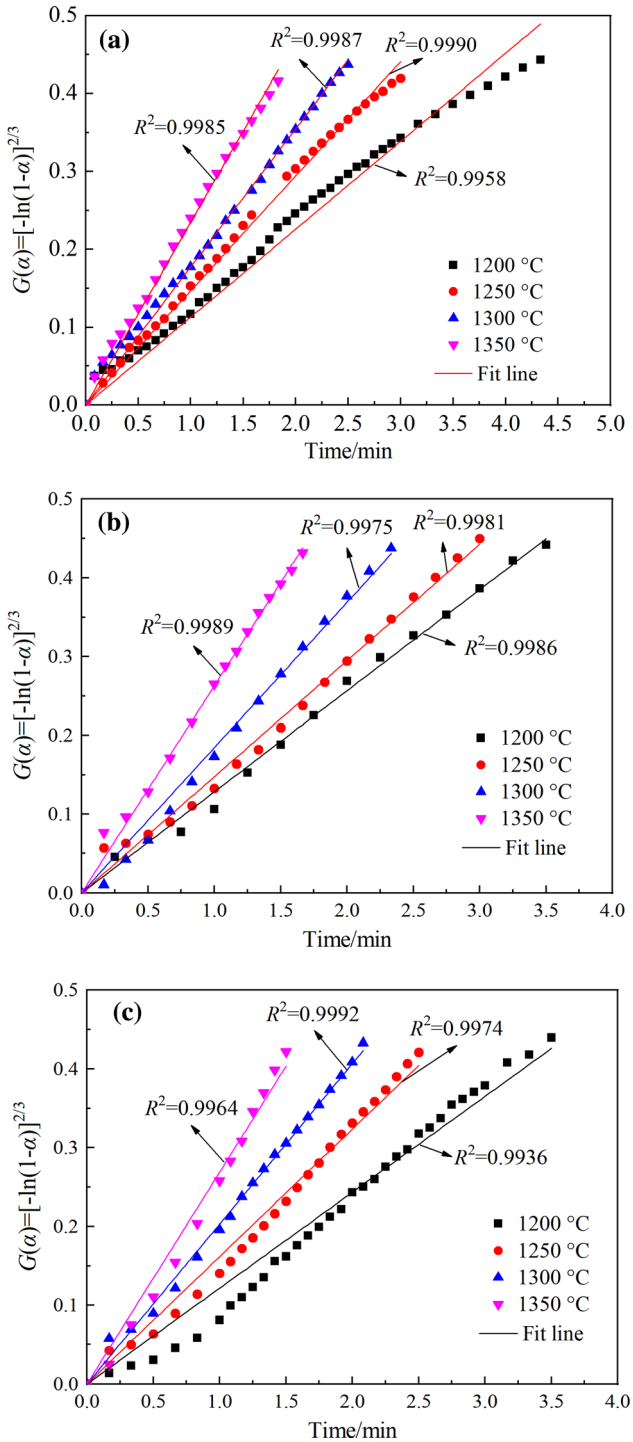

Fig. 9 Linear fitting of $G(\alpha)$ versus time of reaction model at initial stage. **a** C/O = 0.7; **b** C/O = 1.0; **c** C/O = 1.3

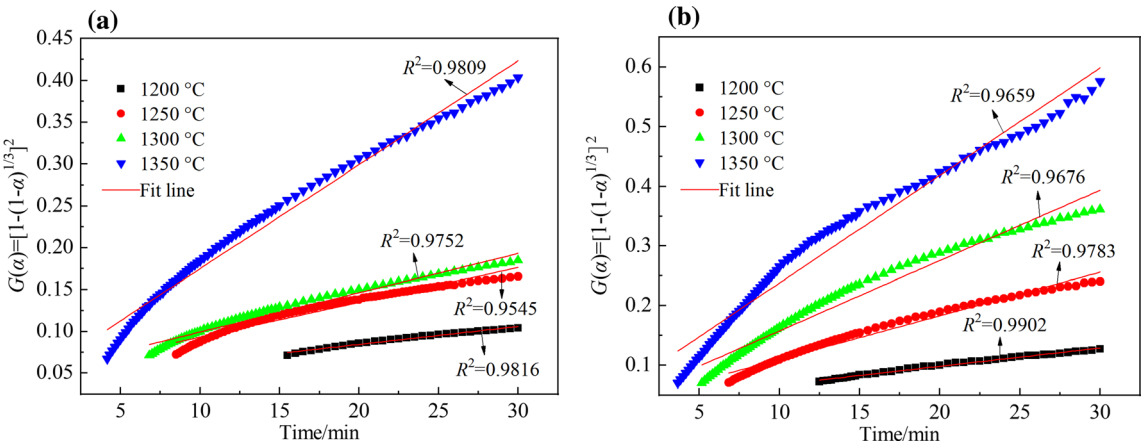

Fig. 10 Linear fitting of $G(\alpha)$ versus time of reaction model at final stage. **a** C/O = 1.0; **b** C/O = 1.3

3 Results and discussion

3.1 Reduction characteristics of HCVTM

To figure out the mass loss of the reduction oxygen and fixed carbon in samples, TG–DSC curves of the mixture of HCVTM and coal were analyzed by NETZSCH STA 409C/CD. TG–DSC curves are shown in Fig. 5. There are three mass loss temperature regions. In the region of 644–985 °C, the DSC curve has an endothermic peak. In this region, the reduction reaction of Fe_3O_4 takes place. In the region of 985–1160 °C, the drastic mass loss appears. In this region, reduction reactions of $FeO{\cdot}TiO_2$ proportionally take place. At 1160–1400 °C, DSC endothermic peaks appear. Deoxidation of Cr_2O_3, V_2O_3, and TiO_2 takes place.

The reduction degree of HCVTM is shown in Fig. 6, when the C/O ratios are 0.7, 1.0, and 1.3 at 1200, 1250, 1300, and 1350 °C, respectively. The tendency of sample reduction degree curves is the same. In the initial reaction region (1–5 min), the reduction degree increased sharply. With the increase in time, in the medium reaction region (5–10 min), the increase rate of reduction degree becomes lower. In the final reaction region (10–30 min), curves level off.

With the increase in C/O ratio and temperature, reduction degree increases obviously. When the temperature is 1350 °C, the reduction degree increases from 0.70 to 0.95. With the increase in temperature, reduction rate and reduction degree rise up to different degrees. When temperature increases from 1200 to 1350 °C, reduction degree increases by 0.15–0.30 with different C/O ratios.

Table 6 Mechanism functions and apparent rate constants at initial stage ($\alpha < 0.25$)

C/O	Temperature/°C	$G(\alpha)$	R^2	$k(T)$/min^{-1}
0.7	1200	$[-\ln(1-\alpha)]^{\frac{2}{3}}$	0.9958	0.1129
	1250		0.9990	0.1470
	1300		0.9987	0.1774
	1350		0.9985	0.2347
1.0	1200	$[-\ln(1-\alpha)]^{\frac{2}{3}}$	0.9986	0.1284
	1250		0.9981	0.1475
	1300		0.9975	0.1845
	1350		0.9989	0.2629
1.3	1200	$[-\ln(1-\alpha)]^{\frac{2}{3}}$	0.9936	0.1218
	1250		0.9974	0.1618
	1300		0.9992	0.2033
	1350		0.9964	0.2690

Table 7 Mechanism functions and apparent rate constants at final stage ($\alpha \geq 0.25$)

C/O	Temperature/°C	$G(\alpha)$	R^2	$k(T)$/min^{-1}
1.0	1200	$\left[1-(1-\alpha)^{\frac{1}{3}}\right]^2$	0.9816	0.0021
	1250		0.9545	0.0041
	1300		0.9752	0.0047
	1350		0.9809	0.0124
1.3	1200	$\left[1-(1-\alpha)^{\frac{1}{3}}\right]^2$	0.9902	0.0030
	1250		0.9783	0.0073
	1300		0.9676	0.0118
	1350		0.9659	0.0180

3.2 Kinetic analysis

Under isothermal conditions, dynamic equation of homogeneous or heterogeneous chemical reactions is expressed as follows:

$$r = \frac{\mathrm{d}\alpha}{\mathrm{d}t} = k(T)f(\alpha) \tag{6}$$

where r is the reduction reaction rate, %/min; α is the conversion ratio of reduction degree, $\alpha = R_t/R_{t1}$; R_{t1} is the final reduction degree; $k(T)$ is the apparent reaction constant, which is a function of reaction temperature T; and $f(\alpha)$ is a function that describes the mechanism of reaction.

After integration, Eq. (6) can be changed into the following form:

$$G(\alpha) = \int_0^{\alpha} \frac{\mathrm{d}\alpha}{f(\alpha)} = \int_0^{t} k(T)\mathrm{d}\tau = k(T)t \tag{7}$$

where $G(\alpha)$ is the reduction reaction rate, %/min.

$G(\alpha)$ has a linear relation with t. The highest linear correlation of $G(\alpha)$ and t is the optimal mechanism function of direct reduction. The slope of the regression line is $k(T)$. The pre-exponential factor and apparent activation energy are obtained by using the logarithmic form of Arrhenius equation as follows:

$$\ln k(T) = \ln A - \frac{E_a}{RT} \tag{8}$$

where R is the universal gas constant, 8.314 J/mol; A is the pre-exponential factor, min^{-1}; and E_a is the activation energy. In this paper, an equal conversion ratio method is applied. The equal conversion ratio method is based on the calculation of the linear correlation of activation energy and reduction degree conversion ratio.

By the equal conversion ratio method, we can get rid of $k(T)$ by the combination of Eqs. (7) and (8)

$$\ln t_\alpha = \ln \frac{G(\alpha)}{A} + \frac{E_a}{RT} \tag{9}$$

where t_α is the reaction time when the conversion ratio is α and temperature is T. Scholars have established many different mechanism functions to describe chemical reactions, which can be summarized as the Avrami-Erofeev equation model, the diffusion model, the power function model, the shrinking core model, and the chemical reaction model. In this paper, 7 kinds of kinetic mechanism functions that are commonly used to describe solid-phase reaction are selected and shown in Table 5. In Table 5, the integral form and differential form of the kinetic mechanism function are all presented.

3.3 Kinetic research of HCVTM direct reduction

In order to determine the optimal kinetic mechanism function, reduction degree and $t/t_{0.5}$ (where $t_{0.5}$ is the time when the conversion ratio is 0.5) are plotted in Fig. 7, based on the experimental data and mechanism functions listed in Table 5. All the experimental data cannot completely accord with a single kinetic mechanism function. Kinetic mechanism changes with the reduction degree, which indicates that the reaction mechanism is complex in the isothermal reduction process. When α is lower than 0.25, the experimental data curve is in accord with mechanism 2 ($A_{3/2}$ model). When the C/O ratio is 0.7 and α is larger than 0.25, experimental data curve is in accord with mechanism 1 (A_1 model), 5 (R_3 model), and 6 (D_6 model). When the C/O ratio is 1.0 and 1.3, α is in the region of 0.25–0.60, experimental data curve is in accord with

Table 8 Correlation coefficients of three modes of C/O ratios (0.7, 1.0, and 1.3) at different stages

C/O	Reduction stage	Temperature/°C	R^2		
			A_1	R_3	D_6
0.7	Final	1200	0.9668	0.9686	0.9884
		1250	0.9701	0.9723	0.9890
		1300	0.9817	0.9795	0.9978
		1350	0.9819	0.9817	0.9977
1.0	Medium	1200	0.9845	0.9775	0.9975
		1250	0.9971	0.9936	0.9983
		1300	0.9951	0.9908	0.9991
		1350	0.9995	0.9977	0.9937
1.3	Medium	1200	0.9825	0.9752	0.9965
		1250	0.9982	0.9953	0.9956
		1300	0.9979	0.9954	0.9963
		1350	0.9978	0.9953	0.9934

mechanisms 1, 5, and 6; when the C/O ratio is 1.0 and α is larger than 0.60, the experimental data curve is in accord with mechanism 6. This means that the reaction mechanism in the isothermal reduction process of HCVTM is changed with the change of C/O ratio and reduction degree.

When the C/O ratio is 0.7, the process of isothermal reduction includes two stages: the initial stage of the reduction ($\alpha \leq 0.25$) and the final stage of reduction ($\alpha > 0.25$). The reaction rate is controlled by the rate of nucleation when $\alpha \leq 0.25$, and the optimal kinetic mechanism function is $G(\alpha) = [-\ln(1-\alpha)]^{2/3}$. The reaction rate is controlled by carbon gasification reaction, phase interface reaction, and three-dimensional diffusion when $\alpha > 0.25$.

When the C/O ratio is 1.0 and 1.3, the process of isothermal reduction includes three stages: the initial stage of reduction ($\alpha \leq 0.25$), the medium stage of reduction ($0.25 < \alpha \leq 0.60$), and the final stage of reduction ($\alpha > 0.60$). Reaction rate is controlled by the rate of nucleation when $\alpha \leq 0.25$, and the optimal kinetic mechanism function is $G(\alpha) = [-\ln(1-\alpha)]^{2/3}$. The reaction rate is controlled by carbon gasification reaction, phase interface reaction, and three-dimensional diffusion when $0.25 < \alpha \leq 0.60$. The reaction rate is controlled by the rate of three-dimensional diffusion when $\alpha > 0.60$, and the optimal kinetic mechanism function is $G(\alpha) = [1-(1-\alpha)^{1/3}]^2$.

The relationship between activation energy and reduction degree is shown in Fig. 8. The activation energy of the three different C/O ratios is almost unchanged when α is less than 0.25, which is about 100 kJ mol^{-1}. Reaction rate is controlled by the growth rate of nucleation. When $\alpha > 0.25$, activation energy gradually increases up to about 200 kJ mol^{-1}. This is owing to the gradual reduction of iron oxides as the reaction is ongoing. In the initial stage, the reduction reaction of HCVTM is Fe_3O_4 and FeO. In the final stage, the main process transforms to $FeTiO_3$ reduction, which is more difficult than the reduction of Fe_3O_4 and FeO.

The dynamic analysis of isothermal reduction process of pellets was carried out by integral method. The linear regression analysis and correlation coefficient of the reduction mechanism function $G(\alpha)$ are shown in Figs. 9 and 10. It indicates that the determined mechanism function has a good linear relation. Linear correlation coefficient R^2 is all above 0.95 at different C/O ratios. Based on the determined optimal mechanism function, we can obtain the apparent rate constant under different temperatures and different C/O ratios conditions, as shown in Tables 6 and 7.

The reduction degree was analyzed by linear regression with the comparison of the medium stage with C/O ratio of 0.7 and the final stage with C/O ratios of 1.0 and 1.3. Results are shown in Table 8. The correlation coefficients

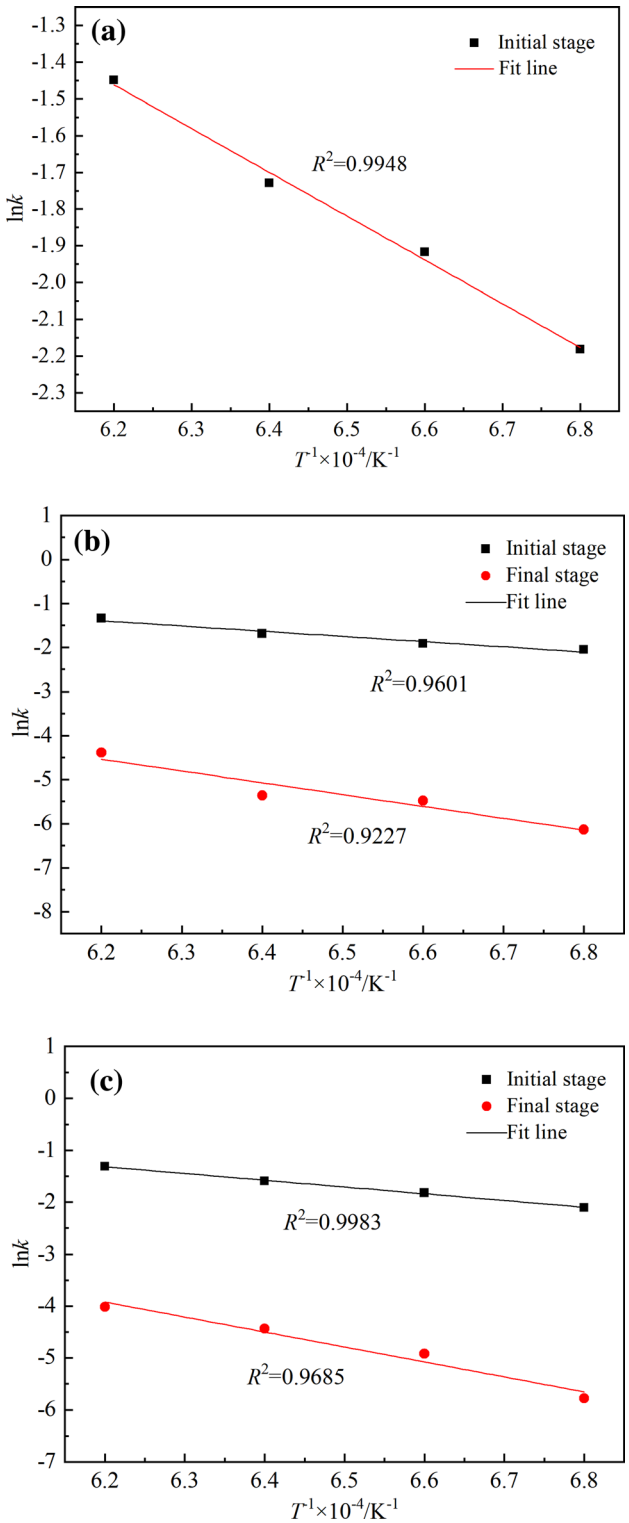

Fig. 11 Linear fitting of ln$k(T)$ versus $1/T$. **a** C/O = 0.7; **b** C/O = 1.0; **c** C/O= 1.3

of the lines were high and close to each other by fitting the experimental data with three models. This illustrates that the mechanism is complex and influenced by the three

Table 9 Kinetic models and parameters of coal-based reduction process

C/O	Stage	Restrictive stage	Kinetic equation	E_a/(kJ mol^{-1})	A/min^{-1}
0.7	Initial	Nucleation and growth	$r = \frac{d\alpha}{dt} = \frac{3}{2} \times A\exp(\frac{-E_a}{RT})(1-\alpha)[-\ln(1-\alpha)]^{\frac{1}{3}}$	99.06	374.44
	Final	–	–	–	–
1.0	Initial	Nucleation and growth	$r = \frac{d\alpha}{dt} = \frac{3}{2} \times A\exp(\frac{-E_a}{RT})(1-\alpha)[-\ln(1-\alpha)]^{\frac{1}{3}}$	98.70	360.95
	Medium	–	–	–	–
	Final	Three-dimensional diffusion	$r = \frac{d\alpha}{dt} = \frac{3}{2} \times A\exp(\frac{-E_a}{RT})(1-\alpha)^{\frac{2}{3}}\left[1-(1-\alpha)^{\frac{1}{3}}\right]^{-1}$	201.8	1.899×10^5
1.3	Initial	Nucleation and growth	$r = \frac{d\alpha}{dt} = \frac{3}{2} \times A\exp(\frac{-E_a}{RT})(1-\alpha)[-\ln(1-\alpha)]^{\frac{1}{3}}$	108.37	356.34
	Medium	–	–	–	–
	Final	Three-dimensional diffusion	$r = \frac{d\alpha}{dt} = \frac{3}{2} \times A\exp(\frac{-E_a}{RT})(1-\alpha)^{\frac{2}{3}}\left[1-(1-\alpha)^{\frac{1}{3}}\right]^{-1}$	223.14	1.185×10^6

models at the medium stage with C/O ratio of 0.7 and at the final stage with C/O ratios of 1.0 and 1.3.

At the same C/O ratio, $k(T)$ increases gradually with the increase in reduction temperature. And $\ln k(T)$ presents a good linear correlation with temperature. Linear fitting of $\ln k(T)$ versus $1/T$ is shown in Fig. 11. And linear correlation coefficient of $\ln k(T)$ with $1/T$ is all above 0.92 at different C/O ratios. At the same C/O ratio and temperature, $k(T)$ at the initial stage is significantly higher than that at the final stage. A and E_a can be calculated, and the results are shown in Table 9.

When the C/O ratio is 1.3, the E_a values of nucleation and growth model and three-dimensional diffusion model are all higher than those with C/O ratios of 0.7 and 1.0. This is because iron oxide is almost completely reduced at the final reduction stage. With the increase in C/O ratio, unreacted carbon increases and hinders mass transfer, which weakens the driving force of the chemical reaction.

Generally speaking, isothermal reduction process of HCVTM has different restrictive stages at different reduction degree. Moreover, in the reduction process, the activation energy is in the range of 99.06–223.14 kJ/mol with different C/O ratios in the experimental conditions.

4 Conclusions

1. With the increase in C/O and temperature, the reduction degree increases obviously. When temperature is 1350 °C, the reduction degree increases from 0.70 to 0.95. When the temperature increases from 1200 to 1350 °C, the reduction degree increases 0.15–0.30 with different C/O ratios.
2. Isothermal reduction process of HCVTM has different restrictive stages at different reduction degrees. When the C/O ratio is 0.7, the reduction process has two stages: the initial stage ($\alpha \leq 0.25$) and the medium stage ($\alpha > 0.25$). When the *C/O* ratio is 1.0 and 1.3, the reduction process has three stages: the initial stage ($\alpha \leq 0.25$), the medium stage ($0.25 < \alpha \leq 0.60$), and the final stage ($\alpha > 0.6$). In the initial stage, the reaction rate is controlled by the growth rate of nuclei, and the optimal kinetic mechanism function is $G(\alpha) = [-\ln(1-\alpha)]^{2/3}$. In the medium stage, the reaction rate is affected by chemical reaction and diffusion without optimal kinetic mechanism function. In the final stage, the reaction rate is controlled by the

three-dimensional diffusion, and the optimal kinetic mechanism function is $G(\alpha) = [1 - (1 - \alpha)^{1/3}]^2$.

3. With the increase in reduction degree, the activation energy decreases slightly and increases gradually from 100 to about 200 kJ mol^{-1} when $\alpha > 0.25$. The apparent rate constant increases gradually with the increase in reduction temperature. $\ln k(T)$ presents a good linear correlation with temperature, and the linear correlation coefficients are all above 0.92 at different C/O ratios.

Acknowledgements The authors will acknowledge the support from the National Natural Science Foundation of China (Nos. 52074081 and 52174319) and the National Key Research and Development Plan (No. 2021YFC2901000).

Conflict of interest We declare that we have no financial and personal relationships with other people or organizations that can inappropriately influence our work; there is no professional or other personal interest of any nature or kind in any product, service and/or company that could be construed as influencing the position presented in, or the review of, the manuscript entitled.

References

[1] J. Tang, M.S. Chu, Z.W. Ying, F. Li, C. Feng, Z.G. Liu, Metals 7 (2017) 153.
[2] J. Tang, M.S. Chu, C. Feng, Y.T. Tang, Z.G. Liu, ISIJ Int. 56 (2016) 210–219.
[3] H.M. Long, T.J. Chun, P. Wang, Q.M. Meng, Z.X. Di, J.X. Li, Metall. Mater. Trans. B 47 (2016) 1765–1772.
[4] X.G. Liu, K.H. Qiu, Q.C. Zhang, Q.M. Ye, C.L. Deng, P.C. Zhang, China Mining Magazine 10 (2001) No. 4, 21–23.
[5] M.L. Hu, L. Liu, X.W. Lv, C.G. Bai, S.F. Zhang, Metall. Mater. Trans. B 45 (2014) 76–85.
[6] J. Fang, Non-blast furnace ironmaking process and theory, Metallurgical Industry Press, Beijing, China, 2002.
[7] X.H. Du, B. Xie, T.P. Lou, J. Northeastern Univ. (Nat. Sci.) 33 (2012) 685–688.
[8] X.J. Liu, D.S. Chen, J.L. Chu, W.J. Wang, Y.L. Li, T. Qi, Rare Met. 41 (2022) 1688–1696.
[9] W. Yu, X.J. Wen, J.G. Chen, J.Z. Kuang, Q.Y. Tang, Y.C. Tian, J.L. Fu, W.Q. Huang, T.S. Qiu, Minerals 7 (2017) 220.
[10] W. Li, G.Q. Fu, M.S. Chu, M.Y. Zhu, Ironmak. Steelmak. 48 (2021) 33–39.
[11] W. Li, G.Q. Fu, M.S. Chu, M.Y. Zhu, Steel Res. Int. 88 (2017) 1600120.
[12] Y.M. Zhang, L.Y. Yi, L.N. Wang, D.S. Chen, W.J. Wang, Y.H. Liu, H.X. Zhao, T. Qi, Int. J. Miner. Metall. Mater. 22 (2017) 504–511.
[13] H.G. Du, Principle of smelting vanadium titanomagnetite in blast furnace, Science Press, Beijing, China, 1996.
[14] X.W. Lv, Z.G. Lun, J.Q. Yin, C.G. Bai, ISIJ Int. 53 (2013) 1115–1119.
[15] L.S. Zhao, L.N. Wang, D.S. Chen, H.X. Zhao, Y.H. Liu, T. Qi, Trans. Nonferrous Met. Soc. China 25 (2015) 1325–1333.
[16] Y.M. Zhang, L.N. Wang, D.S. Chen, W.J. Wang, Y.H. Liu, H.X. Zhao, T. Qi, Int. J. Miner. Metall. Mater. 25 (2018) 131–144.
[17] Y.L. Sui, Y.F. Guo, T. Jiang, G.Z. Qiu, J. Alloy. Compd. 706 (2017) 546–553.
[18] G.G. Liu, Appl. Mech. Mater. 217–219 (2012) 441–444.
[19] Z.F. Yuan, X.Q. Wang, C. Xu, W.B. Li, M. Kwauk, Miner. Eng. 19 (2006) 975–978.
[20] D.S. Chen, B. Song, L.N. Wang, T. Qi, Y. Wang, W.J. Wang, Miner. Eng. 24 (2011) 864–869.
[21] S. Samanta, S. Mukherjee, R. Dey, JOM 67 (2015) 467–476.
[22] S.Y. Chen, M.S. Chu, Int. J. Miner. Metall. Mater. 21 (2014) 225–233.
[23] S. Samanta, M.C. Goswami, T.K. Baidya, S. Mukherjee, R. Dey, Int. J. Miner. Metall. Mater. 20 (2013) 917–924.
[24] Z.J. Liu, G.Q. Yang, Q.G. Xue, J.L. Zhang, T.J. Yang, Chin. J. Process Eng. 9 (2009) No. S1, 51–55.
[25] S.L. Liu, C.G. Bai, T. Hu, X.W. Lv, G.B. Qiu, J. Chongqing Univ. 34 (2011) No. 1, 60–65.
[26] S.L. Liu, C.G. Bai, T. Hu, X.W. Lü, G.B. Qiu, J. Iron Steel Res. 23 (2011) No. 4, 5–8+18.
[27] S. Ding, Q.G. Xue, X.F. She, G. Wang, X.Y. Ning, J.S. Wang, Iron and Steel 49 (2014) No. 8, 15–20.
[28] Y. Sun, H.Y. Zheng, Y. Dong, X. Jiang, Y.S. Shen, F.M. Shen, Int. J. Miner. Process. 142 (2015) 119–124.